Expanded View Figures

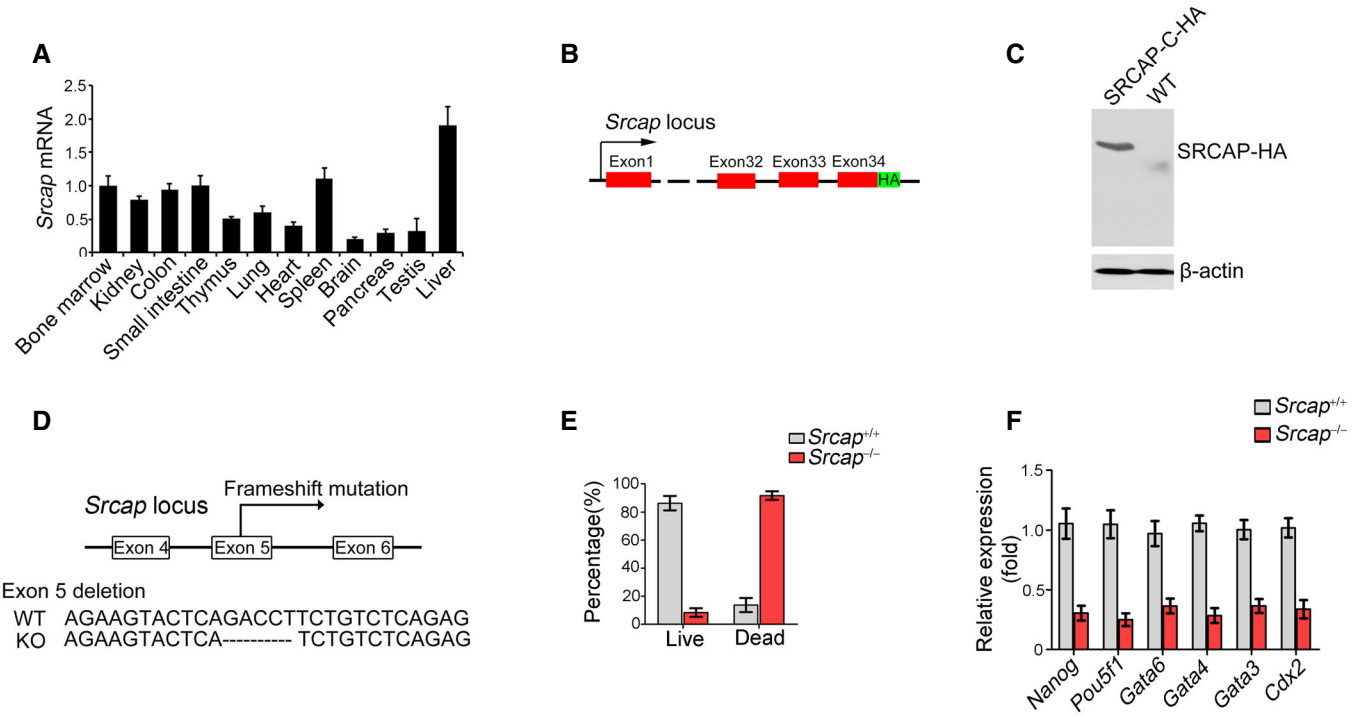

G

Mice	Srcap+/− × Srcap+/− Genotype of newborn pups		
	+/+	+/-	-/-
Total	78(40%)	117(60%)	0(0%)

Figure EV1. Generation strategies of *Srcap* KO mice.

A *Srcap* expression in murine different tissues was examined by real-time PCR. Primers were listed in Table EV1. Relative gene expression folds were normalized to endogenous β-actin and shown as means ± SD. Data represent five independent replicates.

B Schematic diagram of SRCAP-C-HA tag construction for reporter mice.

C Expression of HA-tagged SRCAP protein was confirmed by immunoblotting. β-actin was used as a loading control.

D Schematic diagram of *Srcap* KO construction by CRISPR/Cas9 technology.

E Percentages of live embryos and dead embryos were counted as means ± SD. 200 embryos were isolated and analyzed for each group.

F Expression levels of indicated genes were examined in *Srcap* KO embryos by real-time PCR. Primers were listed in Table EV1. Relative gene expression folds were normalized to endogenous β-actin and shown as means ± SD. Data represent five independent replicates.

G *Srcap*-deficient pups were genotyped after heterozygotes crossing.

Source data are available online for this figure.

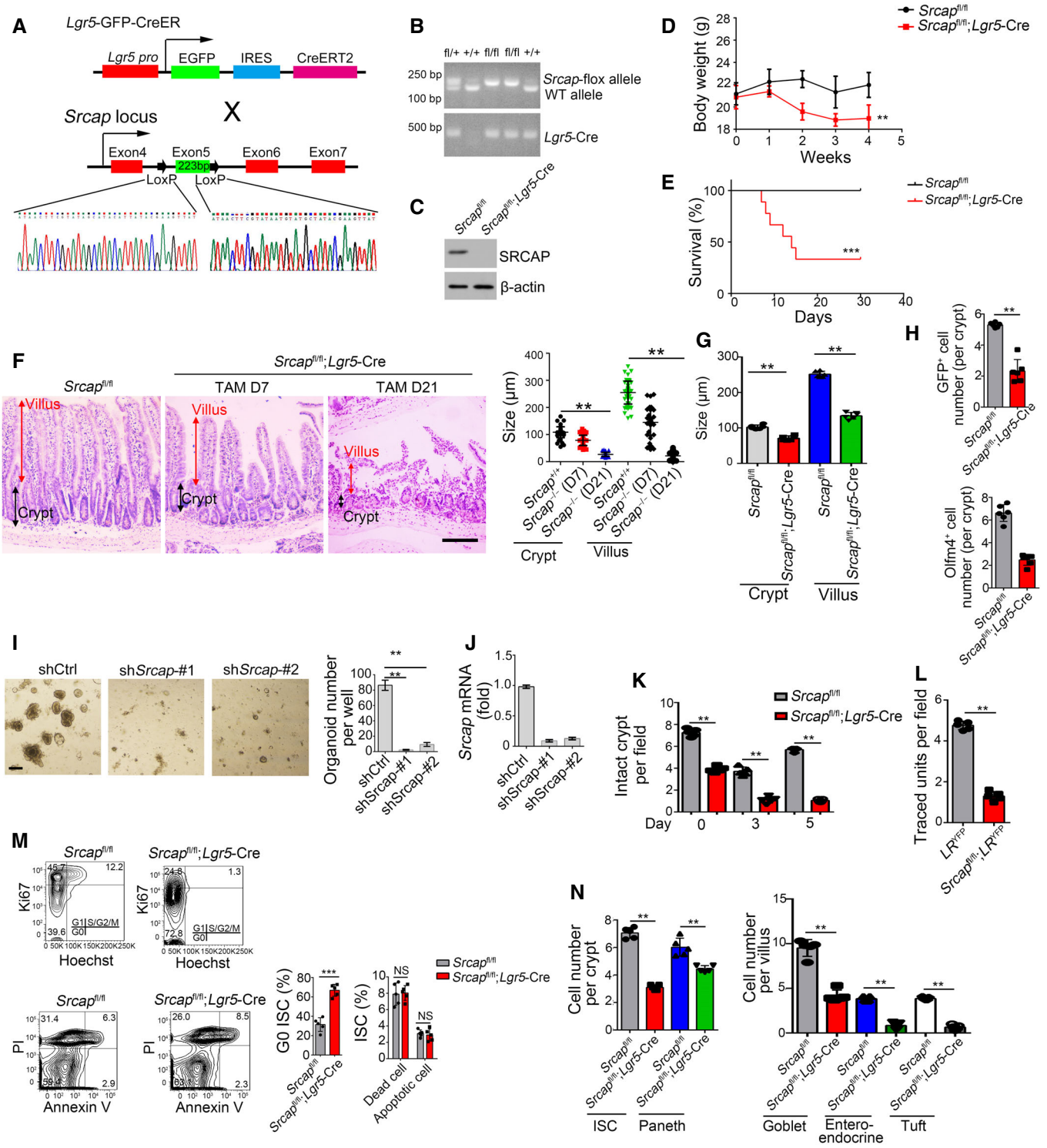
A
Lgr5-GFP-CreER
Lgr5 pro
EGFP
IRES
CreERT2
Srcap locus
X
Exon4
Exon5
223bp
Exon6
Exon7
LoxP
LoxP
B
fl/+ +/+ fl/fl fl/fl +/+
250 bp
100 bp
500 bp
Srcap-flox allele
WT allele
Lgr5-Cre
C
Srcap fl/fl
Srcap fl/fl;Lgr5-Cre
SRCAP
β-actin
D
Srcap fl/fl
Srcap fl/fl;Lgr5-Cre
Body weight (g)
Weeks
**
E
Srcap fl/fl
Srcap fl/fl;Lgr5-Cre
Survival (%)
Days
***
F
Srcap fl/fl
Srcap fl/fl;Lgr5-Cre
TAM D7
TAM D21
Villus
Crypt
Size (μm)
Crypt
Villus
G
Size (μm)
Crypt
Villus
H
GFP+ cell number (per crypt)
Olfm4+ cell number (per crypt)
I
shCtrl
shSrcap-#1
shSrcap-#2
Organoid number per well
J
Srcap mRNA (fold)
K
Srcap fl/fl
Srcap fl/fl;Lgr5-Cre
Intact crypt per field
Day
L
Traced units per field
LRYFP
Srcap fl/fl;LRYFP
M
Srcap fl/fl
Srcap fl/fl;Lgr5-Cre
Ki67
Hoechst
G1
S/G2/M
G0
PI
Annexin V
G0 ISC (%)
ISC (%)
NS
Dead cell
Apoptotic cell
N
Cell number per crypt
ISC
Paneth
Cell number per villus
Goblet
Entero-endocrine
Tuft

Figure EV2. Generation strategies of *Srcap* flox mice.

A Schematic diagram of *Srcap* flox construction by CRISPR/Cas9 technology.
B *Srcap*-deficient pups were genotyped after crossing.
C SRCAP protein was examined in *Srcap*-deleted ISCs by immunoblotting.
D Body weight changes of $Srcap^{fl/fl}$ and $Srcap^{fl/fl}$; $Lgr5^{GFP\text{-}CreERT2}$ mice after TAM treatment were shown as means ± SD. $n = 10$. $^{**}P < 0.01$ by two-tailed Student's *t*-test.
E Kaplan–Meier survival curves of $Srcap^{fl/fl}$ and $Srcap^{fl/fl}$; $Lgr5^{GFP\text{-}CreERT2}$ mice after TAM treatment. $n = 10$. $^{***}P < 0.001$ by log-rank test.
F Representative images of duodenum from 8-week-old $Srcap^{fl/fl}$ and $Srcap^{fl/fl}$; $Lgr5^{GFP\text{-}CreERT2}$ mice after TAM treatment for indicated time ($n = 5$ per group). Scale bar, 100 μm. Length of 100 villi and 100 crypts was measured and shown in right panel as means ± SD. $^{**}P < 0.01$ by two-tailed Student's *t*-test.
G Biological variations and statistical tests were shown as in Fig 2A. Length of villi and crypts (means per mouse) was measured and shown as means ± SD $n = 6$. $^{**}P < 0.01$ by two-tailed Student's *t*-test.
H Biological variations and statistical tests were shown as in Fig 2B. ISC numbers per crypt (means per mouse) were shown as means ± SD $n = 6$. $^{**}P < 0.01$ by two-tailed Student's *t*-test.
I 1×10^4 ISCs were collected and infected with sh*Srcap* lentivirus followed by organoid formation. Typical images of organoid formation were shown in left panel. Scale bar, 200 μm. Organoid numbers per well were counted as means ± SD in right panel. $^{**}P < 0.01$ by two-tailed Student's *t*-test. $n = 6$ for each group.
J *Srcap* was examined in *Srcap*-depleted cells by real-time PCR. Primers were listed in Table EV1. Relative gene expression folds were normalized to endogenous β-actin and shown as means ± SD.
K Biological variations and statistical tests were shown as in Fig 2D. Numbers of intact crypts (means per mouse) were shown as means ± SD $n = 5$. $^{**}P < 0.01$ by two-tailed Student's *t*-test.
L Biological variations and statistical tests were shown as in Fig 2E. Numbers of traced crypt-villus units (means per mouse) were shown as means ± SD $n = 5$. $^{**}P < 0.01$ by two-tailed Student's *t*-test.
M Cell cycle and apoptosis of $Srcap^{+/+}$ and $Srcap^{-/-}$ ISCs were examined by Hoechst/Ki67 and PI/Annexin V FACS and shown in left panel. $n = 6$ mice per group. Percentages of G0 stage ISCs and apoptotic ISCs were counted as means ± SD (right panel). $^{**}P < 0.01$ by two-tailed Student's *t*-test.
N Biological variations and statistical tests showed means per mouse as in Fig 2G. Numbers of each kind of epithelial cells from crypts or villi (means per mouse) were shown in right panel as means ± SD $n = 5$. $^{**}P < 0.01$ by two-tailed Student's *t*-test.

Source data are available online for this figure.

A

Identified protein	Score	Coverage	# Unique peptide	MW (kDa)
Rpl6l	97.94	6.76	1	33.6
REST	88.65	24.40	23	117.7
Tuba1c	78.92	27.39	7	49.9
Tubb5	75.42	36.94	3	49.6
Rps15a	61.93	26.15	2	14.8
Tubb4b	46.37	27.42	1	49.8
Rps3a	44.74	11.74	4	29.9
Parp1	43.03	7.40	5	113.0
Tubb3	41.77	24.22	1	50.4
Tubb2a	41.34	28.09	2	49.9
Myh11	40.39	7.79	13	223.2

B

Identified protein	Sequenced peptides	Coverage
REST	K.VTEGEFVCIFCDR K.GGPEEAGESPAELAALKESAR K.AWESGSSPAEEGEFSK R.QFNCPVCDYAASK R.QEQVLMGVGLVPVR R.EADLLNNAVSNEK K.CNLQYHFK R.VSSSEQNSAMPEGGASHSK K.CDQCNYVASNQHEVTR R.QFNCPVCDYAASKK K.SAQDPPAPPSPSPK K.FFVEESAEKQAK K.GGPEEAGESPAELAALK K.DAEAHPSEEPVNEGPVTK K.CELCPYSSSQK K.KPGSSVSVVQVTTR K.ELPSPVEPAQIEVAQTAPTQVQEEPPPVSEPPR R.CGYNTNR R.VSSSEQNSAMPEGGASHSK K.ELSLLSEMAR K.CNYFSDR K.KFFVEESAEK K.FFVEESAEK K.GNKSAQDPPAPPSPSPK	24.4%

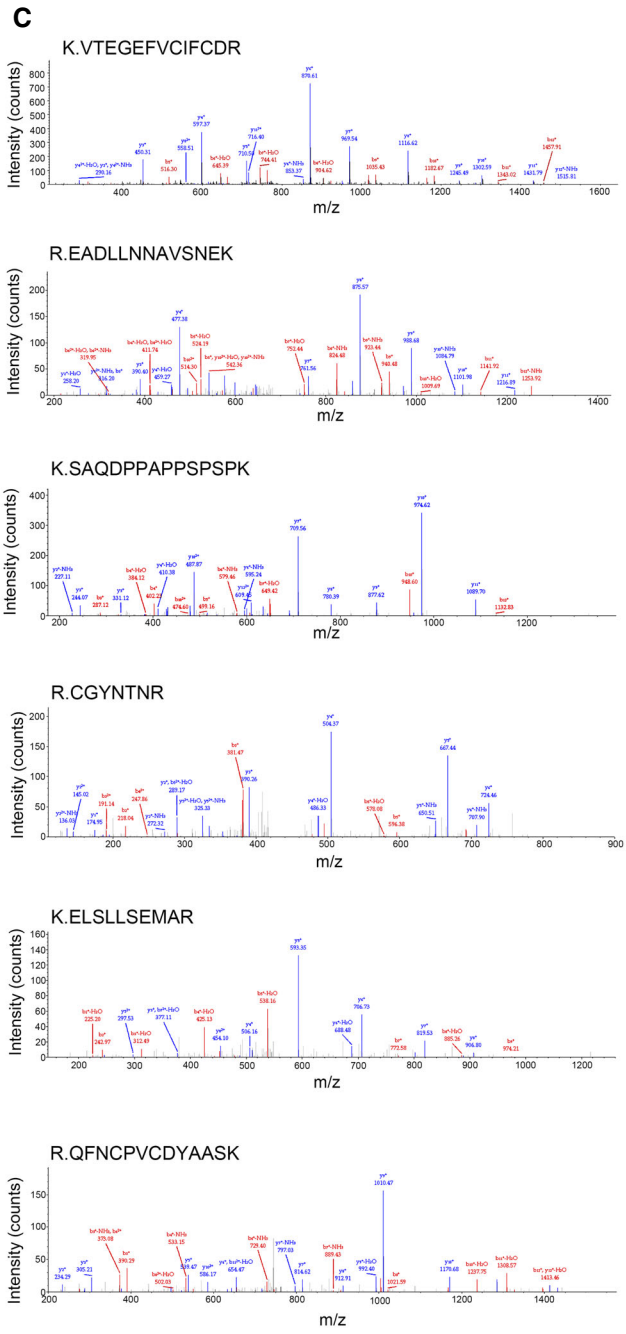

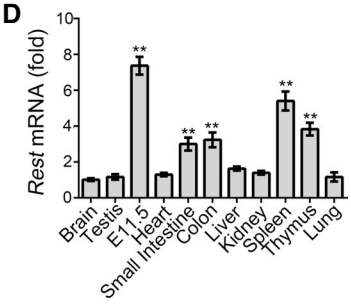

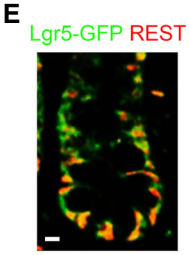

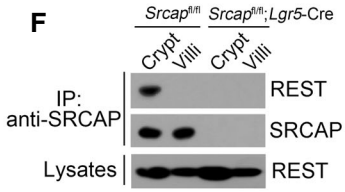

Figure EV3. SRCAP associates with REST.

A–C Identification of Rest as a SRCAP binding protein. Candidate interactors of SRCAP were identified by mass spectrometry LTQ Orbitrap XL.

D *Rest* expression in murine different tissues was examined by real-time PCR. Primers were listed in Table EV1. Relative gene expression folds were normalized to endogenous β-actin and shown as means ± SD. Data represent five independent replicates. $^{**}P < 0.01$ by two-tailed Student's *t*-test.

E Rest expression was visualized in indicated intestinal tissues by immunofluorescence staining. Green: Lgr5-GFP; red: Rest. Scale bar, 10 μm.

F Intestinal crypt and villi lysates were incubated with anti-SRCAP antibody and protein A/G beads in 4°C overnight followed by immunoblotting.

© 2020 The Authors

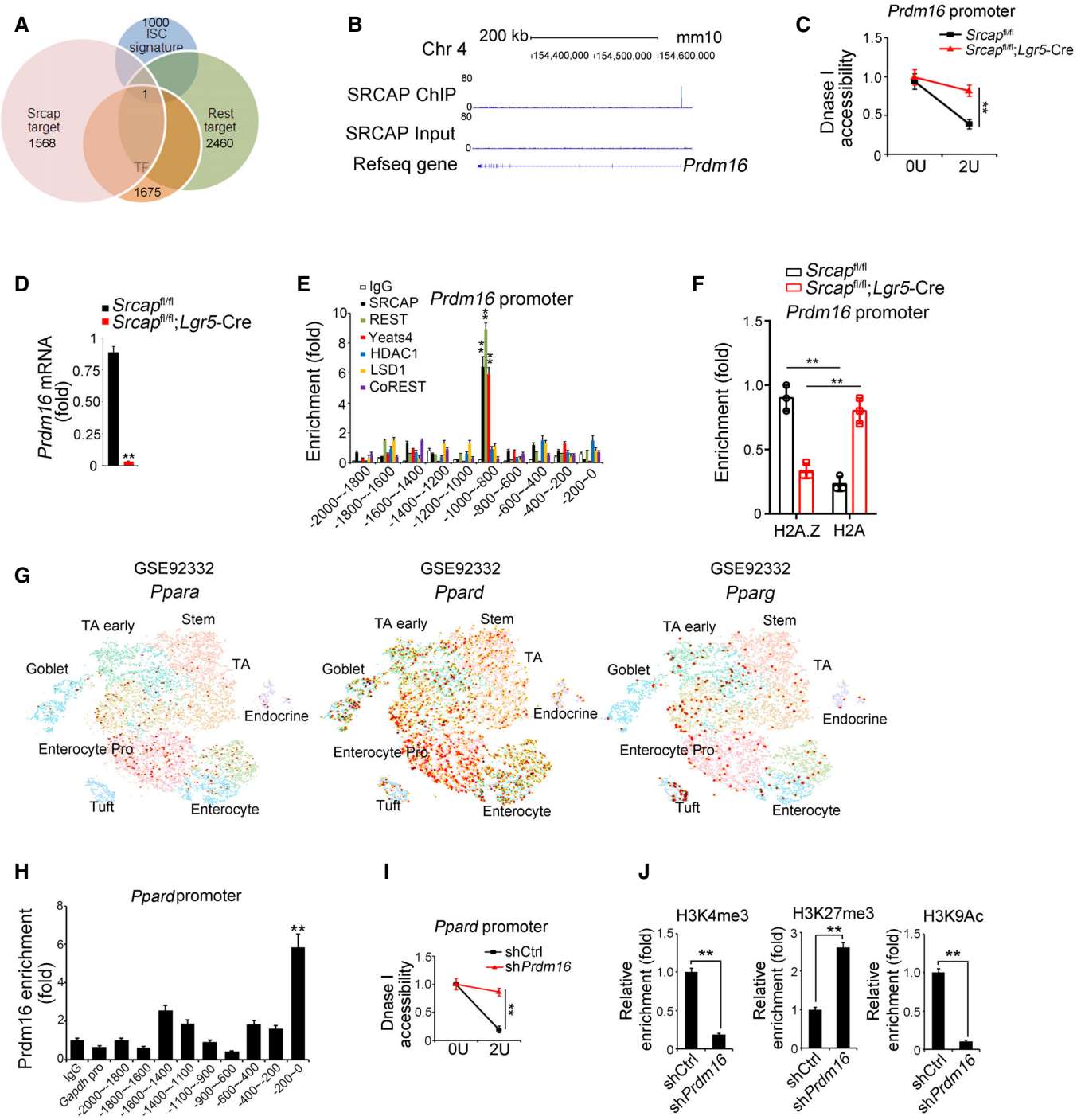

Figure EV4. SRCAP deposits onto Prdm16 promoter for its transcription and activate downstream Ppard expression.

A Target genes of SRCAP and REST in mouse ISCs were analyzed by intersection analysis. Gene clusters of downregulation genes in Srcap KO ISCs, transcriptional factors, genes harbor REST binding site in promoter, and ISC signature genes identified by intestinal epithelium single-cell RNA-seq (GSE92332) were used for analysis. Prdm16 was the only one of SRCAP-targeted TF that harbors REST binding site in its promoter, which was also identified to be one of ISC signature genes by intestinal epithelium single-cell RNA-seq (GSE92332).

B SRCAP deposited to *Prdm16* promoter region near the TSS from ChIP-seq data. *Prdm16* promoter regions from ChIP-seq data were analyzed by IGV software.

C Nuclei were extracted from ISCs followed by DNase I digestion. Total DNA was extracted and quantitated by qPCR with *Prdm16* promoter-specific primers. Primers were listed in Table EV1. Relative fold changes were counted as means ± SD. $^{**}P < 0.01$ by two-tailed Student's *t*-test.

D Prdm16 expression was analyzed by real-time qPCR in $Srcap^{+/+}$ and $Srcap^{-/-}$ ISCs. Primers were listed in Table EV1. Relative gene expression folds were normalized to endogenous β-actin and shown as means ± SD. Data represent five independent replicates. $^{**}P < 0.01$ by two-tailed Student's *t*-test.

E ISCs were lysed for ChIP assays. Indicated proteins enriched to *Prdm16* promoter were examined by real-time qPCR. Signals were normalized to input DNA. Relative fold changes were calculated as means ± SD. Data represent five independent replicates. ** $p < 0.01$ $^{**}P < 0.01$ by two-tailed Student's *t*-test.

F Indicated ISCs were lysed for ChIP assays. H2A.1 and H2A enriched to *Prdm16* promoter were examined by real-time qPCR. Signals were normalized to input DNA. Relative fold changes were calculated as means ± SD. Data represent five independent replicates. $^{**}P < 0.01$ by two-tailed Student's *t*-test.

G Expression levels and patterns of PPAR components in murine intestinal epithelium were analyzed based on a single-cell RNA-seq dataset (GSE92332).

H Prdm16 was recruited near the TSS region of *Ppard* promoter in ISCs. ISCs were lysed for ChIP assay with anti-Prdm16 antibody. Prdm16 protein enriched to *Ppard* promoter was examined by real-time qPCR. Signals were normalized to input DNA. Primers were listed in Table EV1. IgG and Prdm16 proteins enriched on *Gapdh* promoter were used as negative controls. Relative fold changes were calculated as means ± SD. Data represent five independent replicates. $^{**}P < 0.01$ by two-tailed Student's *t*-test.

I Nuclei were extracted from ISCs followed by DNase I digestion. Total DNA was extracted and quantitated by qPCR with *Ppard* promoter-specific primers. Primers were listed in Table EV1. Relative fold changes were counted as means ± SD. $^{**}P < 0.01$.

J ISCs were lysed for ChIP assay. Indicated proteins enriched to *Ppard* promoter were examined by real-time qPCR. Signals were normalized to input DNA. Enrichment fold changes were counted as means ± SD. Data represent five independent replicates. $^{**}P < 0.01$ by two-tailed Student's *t*-test.

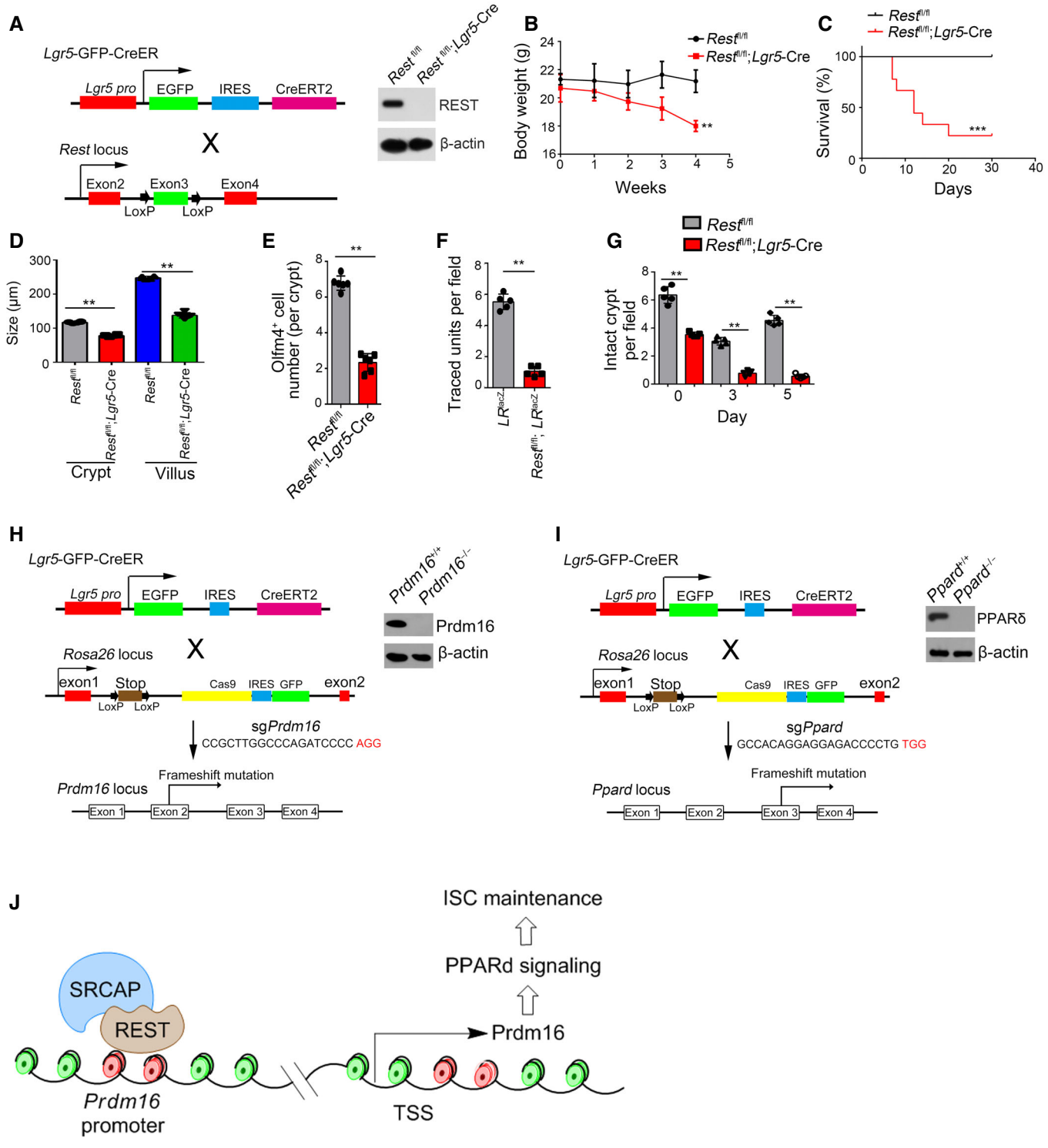

Figure EV5. Generation strategies of *Rest* KO, *Prdm16* KO and *Ppard* KO mice. Generation strategies of *Rest* KO, *Prdm16* KO and *Ppard* KO mice.

A Schematic diagram of *Rest* KO mice and validation by immunoblotting.
B Body weight changes of $Rest^{fl/fl}$ and $Rest^{fl/fl}$; $Lgr5^{GFP\text{-}CreERT2}$ mice after TAM treatment were shown as means ± SD $n = 10$. $^{**}P < 0.01$ by two-tailed Student's *t*-test.
C Kaplan–Meier survival curves of $Rest^{fl/fl}$ and $Rest^{fl/fl}$; $Lgr5^{GFP\text{-}CreERT2}$ mice after TAM treatment. $n = 10$. $^{***}P < 0.001$ by log-rank test.
D Biological variations and statistical tests were shown as in Fig 6A. Length of villi and crypts (means per mouse) was measured and shown as means ± SD $n = 6$. $^{**}P < 0.01$ by two-tailed Student's *t*-test.
E Biological variations and statistical tests were shown as in Fig 6C. $OLFM4^{+}$ ISC numbers per crypt (means per mouse) were shown as means ± SD $n = 6$. $^{**}P < 0.01$ by two-tailed Student's *t*-test.
F Biological variations and statistical tests were shown as in Fig 6E. Numbers of traced crypt-villus units (means per mouse) were shown as means ± SD $n = 5$. $^{**}P < 0.01$ by two-tailed Student's *t*-test.
G Biological variations and statistical tests were shown as in Fig 6F. Numbers of intact crypts (means per mouse) were shown as means ± SD $n = 5$. $^{**}P < 0.01$ by two-tailed Student's *t*-test.
H Schematic diagram of *Prdm16* KO by CRISPR/Cas9 technology and validation by immunoblotting.
I Schematic diagram of *Ppard* KO by CRISPR/Cas9 technology and validation by immunoblotting.
J A work model represents the mechanism of SRCAP regulating ISC self-renewal. SRCAP recruits REST protein onto the *Prdm16* promoter to induce its transcription, which promotes PPAR-δ signaling activation that maintains ISC self-renewal.

Source data are available online for this figure.